Deregulations of miR-1 and its target Multiplexin promote dilated cardiomyopathy associated with myotonic dystrophy type 1

Anissa Souidi[1], *Masayuki Nakamori*[2], *Monika Zmojdzian*[1], *Teresa Jagla*[1], *Yoan Renaud*[1] *and Krzysztof Jagla*[1]

[1] iGReD Genetics Reproduction and Development Institute, Clermont Auvergne University, France
[2] Department of Neurology, Osaka University Graduate School of Medicine, Suita 565-0871, Osaka, Japan

Abstract

Myotonic dystrophy type 1 (DM1) is the most common muscular dystrophy. It is caused by the excessive expansion of non-coding CTG repeat, which when transcribed affect functions of RNA-binding factors. Specifically, MBNL1 is sequestered in nuclear foci while CELF1 is stabilised, with adverse effects on alternative splicing, processing and stability of a large set of muscular and cardiac transcripts. Among these effects, inefficient processing and down-regulation of muscle- and heart-specific miRNA, *miR-1*, has been reported in DM1 patients, but the impact of reduced *miR-1* on DM1 pathogenesis was unknown. Here, we used *Drosophila* DM1 models to explore *miR-1* involvement in cardiac dysfunction in DM1. We found that *miR-1* down-regulation in the heart led to dilated cardiomyopathy (DCM), a DM1-associated phenotype. We then combined *in silico* screening for *miR-1* targets with transcriptional profiling of DM1 cardiac cells to identify *miR-1* target genes with potential roles in DCM. We identified *Multiplexin* (*Mp*) as a new cardiac *miR-1* target involved in DM1. Mp and its human ortholog Col15A1 were both highly enriched in cardiac cells of DCM-developing DM1 flies and in heart samples from DM1 patients with DCM, respectively. Importantly, when overexpressed in the heart, Mp induced DCM, whereas its attenuation ameliorated the DCM phenotype in aged DM1 flies. Reduced levels of *miR-1* and consecutive up-regulation of its target *Mp/Col15A1* are thus critical in DM1-associated DCM.

Introduction

Myotonic dystrophy type 1 (DM1) is the most common muscular dystrophy in adults, with an estimated incidence of one in 8000 births (Meola and Cardani, 2015). DM1 is a multisystem disorder, with cardiac abnormalities accounting for 30% of fatalities (Mathieu et al., 1999). Cardiac involvements in DM1 include conduction defects, supraventricular and ventricular arrhythmias (Pelargonio et al., 2002), impaired diastolic or systolic function (Hermans et al., 2012; Pelargonio et al., 2002) and dilated cardiomyopathy (DCM) (Hermans et al., 2012; Lin et al., 1989; Harold H. Nguyen et al., 1988; Papa et al., 2018; Schilling et al., 2013).

The primary cause of DM1 is gain-of-function of toxic transcripts carrying expanded non-coding CUG repeats that aggregate into foci in nuclei, sequestering RNA-binding protein Muscleblind-like 1 (MBNL1) (Fardaei et al., 2002, 2001). Reduced MBNL1 levels and concomitant stabilisation of another RNA-binding protein, CELF1 (Kuyumcu-Martinez et al., 2007), lead to deregulation of alternative splicing, with abnormal expression of embryonic splice variants in adult tissues (Lee and Cooper, 2009). For example, CELF1-dependent inclusion of fetal exon 5 in the adult isoform of *cardiac troponin T* (*cTnT*) has been associated with cardiac conduction defects in DM1 (Philips et al., 1998). Besides their roles as alternative splicing regulators, both MBNL1 and CELF1 are involved in mRNA translation (Dasgupta and Ladd, 2012; de Haro et al., 2013; Timchenko et al., 2006, 2005), de-adenylation and decay (Dasgupta and Ladd, 2012; Masuda et al., 2012; Vlasova et al., 2008), and in RNA editing (Dasgupta and Ladd, 2012). MBNL1 is specifically involved in miRNA processing (Rau et al., 2011). These diverse functions of MBNL1 and CELF1 mean that DM1 may involve deregulation of multiple pathways.

To investigate the pathophysiology and the molecular mechanisms underlying DM1, several DM1 models, both mouse (Huguet et al., 2012; Orengo et al., 2008; Wang et al., 2007) and *Drosophila* (de Haro et al., 2006; Garcia-Lopez et al., 2008; Houseley et al., 2005; Picchio et al., 2013), have been created.

Reduction of MBNL1 and stabilisation of CELF1 is thought to be involved in most DM1 phenotypes. Indeed, *Mbnl1* knockout mice develop muscle myotonia, weakness/wasting and cardiac defects including dilated cardiomyopathy and heart conduction block (Lee et al., 2013). Mice overexpressing *CELF1* in the heart show conduction abnormalities and dilated cardiomyopathy (Koshelev et al., 2010) thus confirming the contribution of MBNL1

sequestration and CELF1 upregulation to DM1 pathogenesis. Overall, the mouse models reproduced multiple DM1 features including RNA foci formation and various alternative splice defects.

We generated a series of inducible *Drosophila* DM1 lines bearing UAS-iCTG constructs with 240, 480, 600 and 960 CTGs (Picchio et al., 2013). These lines were used to model DM1 in larval somatic muscles showing not only nuclear foci formation and Mbl sequestration but also muscle hypercontraction, splitting of muscle fibres, reduced fibre size and myoblast fusion defects leading to impaired larva mobility (Picchio et al., 2013). The severity of phenotypes in these *Drosophila* models could be correlated with repeat size (Picchio et al., 2013), as also observed in DM1 patients. Finally, the overexpression of *Drosophila CELF1* ortholog *Bru-3* and attenuation of *MBNL1* counterpart *mbl* (Picchio et al., 2018; Auxerre-Plantié et al., 2019) offer further valuable models for identifying gene deregulations underlying DM1.

Among molecular mechanisms associated with DM1, deregulation of miRNAs and in particular reduced levels of evolutionarily conserved muscle- and heart-specific miRNA, *miR-1,* has been reported in DM1 patients (Rau et al., 2011) and in DM1 models including mouse (Kalsotra et al., 2014) and *Drosophila* (Fernandez-Costa et al., 2013). However, the impact of *miR-1* down-regulation on DM1-associated phenotypes has not yet been analysed.

Here, we made use of *Drosophila* DM1 models to explore *miR-1* involvement in cardiac dysfunction in DM1. We observed that *dmiR-1* level was reduced in the cardiac cells of DM1 flies and that its down-regulation in the heart led to DCM, thus suggesting that reduced *dmiR-1* levels contribute to DM1-associated DCM. Among potential *dmiR-1* regulated genes from *in silico* screening, we identified *Multiplexin* (*Mp*) / *Collagen15A1* (*Col15A1)* as a new cardiac *dmiR-1* target involved in DM1. Both Mp and Col15A1 proteins were highly enriched in cardiac cells of DCM-developing DM1 flies and in heart samples from DM1 patients with DCM, respectively. Moreover, heart-targeted overexpression of Mp was sufficient to induce DCM, whereas its attenuation ameliorated the DCM phenotype in DM1 flies. *miR-1* and its target *Mp/Col15A1* thus emerge as molecular determinants of DM1-associated DCM.

Results

Heart-targeted *dmiR-1* attenuation causes DCM in *Drosophila*

Reduced *miR-1* levels had previously been observed in mice developing DCM (Isserlin et al., 2014) and in cardiac samples from patients with end-stage DCM (Ikeda et al., 2007). It had also been shown that *miR-1* knockout mice display the DCM phenotype (Wei et al., 2014). However, whether *miR-1* attenuation specifically within the heart leads to DCM has not been assessed. Here we tested heart-specific knockdown (KD) of *dmiR-1* in *Drosophila* using a sponge system (Fulga et al., 2015). In the *Hand>dmiR-1KD* context, the adult fly hearts showed a larger diameter with an enlarged cardiac lumen (Fig. 1A, B). Consistent with this observation, analyses of semi-intact *Hand>dmiR-1-KD* heart preparations and generated M-modes (Fig.1C) confirmed enlargement of the cardiac tube and showed significantly increased diastolic and systolic heart diameters (Fig. 1D, E). We then characterized the effects of *dmiR-1* down-regulation on heart contractility by assessing percent fractional shortening (%FS), which refers to the size of the cardiac tube at the end of systole and diastole. The cardiac dilation in *Hand>dmiR-1-KD* flies was associated with a significant reduction in heart contractility (Fig. 1F). *dmiR-1* attenuation in the *Drosophila* heart thus leads to DCM.

DM1 flies develop a DCM phenotype and show a reduced *dmiR-1* level in cardiac cells

DCM accounts for fatal cardiac involvements in DM1 patients, but the gene deregulations underlying DM1-associated DCM have not been identified. To address this issue, we first tested whether *Drosophila* DM1 models developed DCM. In three heart-specific DM1 contexts, namely (i) overexpression of 960CTG repeats, (ii) overexpression of *CELF1* orthologue *Bru3*, and (iii) attenuation of *MBNL1* orthologue *mbl*, the DCM phenotype was present in *Hand>Bru3* and *Hand>mblRNAi* models (Fig. 2A,B,C,D,E,F) but not in *Hand>960CTG* (Fig. S1A,B,C).

Given that *dmiR-1* attenuation leads to DCM and that *Hand>Bru3* and *Hand>mblRNAi* DM1 models develop a DCM phenotype, we tested whether cardiac cells of *Hand>Bru3* and *Hand>mblRNAi* flies showed reduced *dmiR-1* levels. Using single molecule fluorescence *in situ* hybridisation (smFISH), we found a significantly reduced *dmiR-1* level in cardiac cells of both DCM-developing DM1 contexts (Fig. 2G,H,I and Fig. S2). *Pre-miR-1* expression was also lower in young DM1 flies (Fig. S1D), whereas hearts from aged *Hand>mblRNAi* flies showed an increased *pre-miR-1* level, most probably owing to impaired processing

(Fig. S1D). DCM-developing *Drosophila* DM1 models could thus serve to test and identify genes deregulated in the DM1-associated DCM context in response to a reduced *dmiR-1* level.

dmiR-1 target Multiplexin is up-regulated in DCM-developing DM1 flies

To identify *dmiR-1* target genes involved in DM1-associated DCM, we first performed *in silico* screening by mapping *Drosophila*-specific *dmiR-1* seed sites annotated in miRBase (Griffiths-Jones et al., 2006; http://www.mirbase.org/) on 3'UTR regions of *Drosophila* genes up-regulated in two DCM-developing DM1 contexts (Table 1; Fig. 3A) (Auxerre-Plantié et al., 2019). We identified a set of candidate genes, of which *Multiplexin (Mp)* (Table 1, scheme in Fig. 3A).

Mp, a *Drosophila* ortholog of mammalian Collagen XVIII and Collagen XV, belongs to the family of multi-domain collagens. It is composed of an N-terminal thrombospondin-related domain, followed by multiple Collagen repeats, a Collagen trimerisation domain and a C-terminal endostatin domain (Meyer and Moussian, 2009). Mp also contains consensus glycosaminoglycan (GAG) attachment sites, and biochemical analysis of the protein extracted from embryonic tissues revealed the presence of chondroitin sulphate (CS) chains, making it more like human collagen XV than collagen XVIII in this respect. In the embryonic *Drosophila* heart, Mp is expressed in cardioblasts of the heart proper but not in aorta (Harpaz et al., 2013; Meyer and Moussian, 2009). The Mp was shown to be deposited in a polarised way along the heart lumen during cardiac tube formation (Meyer and Moussian, 2009) and involved in lumen shaping by enhancing Slit/Robo activity (Harpaz et al., 2013).

Here, we show that Mp is also expressed in the adult fly heart (Fig. S3B,B',B''). Consistent with the predicted location of an extracellular matrix protein, Mp was detected on the luminal and external surfaces of the cardiomyocytes ensuring cardiac contractions and was also present on the underlying adult heart ventral longitudinal muscles (VLM) (Fig. S3B,B').

The predicted *dmiR-1*-binding site within the *Mp*-3'UTR region (Fig. 3B) is expected to negatively regulate *Mp* transcript level in the presence of *dmiR-1*. To assess the biological relevance of this binding site *in vivo*, we cloned the *Mp-3'UTR* fragment carrying the *dmiR-1* seed site downstream of the GFP coding sequence to generate the *UAS-GFP-Mp3'UTR* transgenic line. In parallel, the *UAS-GFP-ΔMp3'UTR* line was created in which the *dmiR-1* biding site was deleted from the 3'UTR *Mp* sequence. Both GFP sensor lines were then combined with the *UAS-dmiR-1* line to generate double transgenic lines *UAS-GFP-Mp3'UTR;*

UAS-dmiR-1 (Fig. 3C, D) and *UAS-GFP-ΔMp3'UTR*; *UAS-dmiR-1* (Fig. 3E, F), respectively. We found that expression of *dmiR-1* in *Hand>GFP-3'UTRMp* hearts significantly reduced the GFP signal in cardiac and pericardial cells (Fig. 3D'), suggesting that *dmiR-1* binds to the predicted seed site and negatively regulates *Mp* mRNA expression in the adult fly heart. The deletion of the *dmiR-1* binding site in *Hand>GFP-Δ3'UTRMp; dmiR1* heart prevented the repressive effects of *dmiR-1* (Fig. 3F'), demonstrating that the GFP silencing observed in *Hand>GFP-Mp3'UTR; dmiR1* hearts (Fig. 3D') is *dmiR-1* dependent. This finding is also consistent with an increased Mp protein levels detected in hearts of the *Hand>miR-1-sponge* context mimicking *miR-1* attenuation and leading to DCM (Fig. S3J).

We then tested whether Mp protein level increased in DM1 contexts with DCM characterised by a reduced *dmiR-1*. We detected a significant increase in Mp protein level on the surface of cardiomyocytes in DCM-developing lines (*Hand>mblRNAi* and *Hand>Bru3*) in both young and aged flies (Fig. 3G,H,I,J,K,L). A similar increase in Mp expression was found in DM1 pericardial cells (Fig. S3D',E',F',G',H,I).

Heart-targeted Mp overexpression leads to DCM in aged flies

Mp protein level increases in DCM-developing DM1 hearts and in the heart-specific *dmiR-1* attenuation context causing DCM. Moreover, the 3'-UTR region of *Mp* carries a *dmiR-1* binding site, making Mp an *in vivo dmiR1* target in the heart. All these observations prompted us to determine whether the increased cardiac Mp level could lead to DCM. To generate cardiac Mp gain-of-function we crossed *Hand-Gal4* with the *UAS-3HNC1 (UAS-Mp)* line (Meyer and Moussian, 2009). The *Hand>3HNC1* adult flies expressed a high Mp protein level in the heart (Fig. 4B,D). Already at age one week, the Mp gain-of-function flies displayed a larger heart tube diameter and a wider cardiac lumen than controls (*UAS-3HNC1)* (Fig. 4D). The diastolic and systolic diameters of hearts overexpressing Mp were also significantly increased relative to controls (Fig. 4E,F). However, cardiac contractility was not affected (Fig. 4G). In contrast, the five-week-old *Hand>3HNC1* flies, besides an increase in systolic and diastolic diameters (Fig. 4E,F,H,H'), showed significantly reduced fractional shortening and thus adversely affected cardiac contractility (Fig. 4G). These findings demonstrate that heart-specific increase in Mp protein level is detrimental to cardiac function, leading to DCM in aged flies.

To further analyse effects of Mp expression level on heart morphology and function, we tested the impact of cardiac-specific Mp knockdown at ages one and five weeks. We observed a reduced heart lumen in *Hand>MpRNAi* flies compared to controls and a significant decrease in diastolic and systolic diameters at ages one and five weeks, with no influence on cardiac contractility (Fig. S4).

Taken together, our findings demonstrate that Mp expression level plays a critical role in setting the size of the cardiac lumen and the systolic and diastolic fly heart variables, and its overexpression in the heart leads to DCM. We thus infer that the reduced *dmiR-1* leading to the up-regulation of its direct target Mp promotes development of DCM in the DM1 context (see scheme in Fig. 4I).

Mp counterpart Col15A1 is up-regulated in cardiac samples of DM1 patients with DCM

Given the increased Mp level in DM1 fly models developing DCM, we examined whether expression of its human ortholog Col15A1 was also up-regulated in cardiac cells of DM1 patients. Of three DM1 cardiac tissue samples tested, two were from DM1 patients with DCM (Fig. 5A,B). At both RNA and protein levels, DM1 cardiac cells showed an increase in Col15A1 expression compared to cardiac cells from healthy donors, with differentially higher Col15A1 levels in DM1 patients with DCM compared to cardiac cells from DM1 patient without DCM (Fig. 5A,B). Thus, like Mp in *Drosophila* DM1 models, the up-regulation of Col15A1 in the heart correlates with DCM in DM1 patients.

Heart-specific attenuation of Mp ameliorates DM1-associated DCM phenotype

To determine whether the increased Mp/Col15A1 levels could contribute to the DCM phenotype in DM1, we applied our DM1 fly models and performed genetic rescue experiments by attenuating Mp expression in the DCM-developing *Hand>Bru3* context. In young one-week-old flies, heart-specific Mp attenuation had no effect on diastolic or systolic diameters, nor on contractility of *Hand>Bru3* hearts (Fig. S5). However, in five-week-old *Hand>Bru3; MpRNAi* flies, the systolic and diastolic diameters were reduced (Fig. 5C,D), associated with a significant increase in the fractional shortening variable compared to the aged DM1 context (Fig. 5E). However, rescue remained partial compared to aged control flies (Fig. 5E). Heart-specific attenuation of Mp thus improves DCM phenotype in aged DM1 flies.

Discussion

Myotonic dystrophy type 1 is the most common muscular dystrophy in adults. Cardiac repercussions including DCM are among the main causes of death in DM1 (Groh et al., 2008). However, the underlying mechanisms remain poorly understood, impeding the development of adapted treatments. As we previously demonstrated (Auxerre-Plantié et al., 2019; Souidi et al., 2018; Souidi and Jagla, 2021), *Drosophila* DM1 models recapitulate all the cardiac phenotypes observed in DM1 patients and so could help gain insight into gene deregulations underlying DM1-associated DCM.

DM1 fly models show reduced *dmiR-1* in cardiac cells and develop DCM

In humans, DCM is characterized by left ventricular dilation and systolic dysfunction defined by a depressed ejection fraction. Similarly, in DCM-developing flies, the cardiac tube is enlarged and shows an increased diastolic and systolic diameter with reduced contractility. The loss of cardiac miRNAs and in particular *miR-1* has already been correlated to DCM and heart failure in mice (Rao Prakash et al., 2009; Wei et al., 2014) and observed in patients with end-stage DCM (Ikeda et al., 2007). It is well known that *miR-1* regulates genes involved in cardiac development and function including *Nkx2.5*, *SRF* and components of *WNT* and *FGF* signalling pathways (Kura et al., 2020) and that its level is reduced in the pathological context of DM1 (Rau et al., 2011). However, it was not known whether the low *miR-1* level caused DM1-associated DCM, nor what were the downstream *miR-1* targets. Here, we show that two heart-targeting *Drosophila* DM1 models, *Hand>mblRNAi* and *Hand>Bru3* mimicking sequestration of MBNL1 and stabilisation of CELF1, respectively, developed DCM and showed a reduced expression of *dmiR-1* in cardiac cells. Because overexpression of CELF1 (Koshelev et al., 2010) and loss of MBNL1 (Lee et al., 2013) also result in DCM in mice, *Drosophila* appears well-suited to assessing the impact of reduced *miR-1* in DM1-associated DCM. One mechanism explaining why *miR-1* levels fall in the DM1 context is the sequestration of MBNL1, which can no longer play its physiological role in *pre-miR-1* processing into mature *miR-1* (Rau et al., 2011). Here, we observed reduced *dmiR-1* also upon cardiac overexpression of CELF1 ortholog Bru3. How CELF1/Bru3 impinges on *miR-1* levels is not fully understood, but the fact that CELF1 could bind UG-rich miRNAs and mediate their degradation by recruiting poly(A)-specific ribonuclease (PARN) (Katoh et al., 2015) could explain reduced *dmiR-1* levels in the *Hand>Bru3* context. Given that both *Drosophila* DM1 models developing DCM showed markedly reduced *dmiR-1* in cardiac cells, we sought

to determine whether heart-targeted attenuation of *dmiR-1* was sufficient to induce DCM: *dmiR-1* knockdown in the heart mimics DM1-associated DCM.

Col 15A1 ortholog Mp is a new *miR-1* target involved in DM1-associated DCM

To identify candidate *dmiR-1* target genes involved in DCM we performed *in silico* screening for *dmiR-1* seed sites in the 3'UTR regions of genes up-regulated in cardiac cells from DM1 models (Auxerre-Plantié et al., 2019) developing DCM (see Table 1). Among 1189 3'UTR sequences tested we found that 162 bore potential *dmiR-1* seed sites, of which the 3'UTR of *Multiplexin* (*Mp)*. *Mp* codes for extracellular matrix protein belonging to a conserved collagen XV/XVIII family. We top-ranked *Mp* because of its known role in setting the size of the cardiac lumen (Harpaz et al., 2013). The *Mp-/-* embryos were found to present a narrower lumen with reduced contractility of the heart tube (Harpaz et al., 2013), whereas the mouse mutants of *Mp* ortholog, *Col15A1,* showed age-related muscular and cardiac deteriorations linked to a degraded organisation of the collagen matrix (Eklund et al., 2001; Rasi et al., 2010). This prompted us to examine how Mp was expressed in the adult fly heart and what the effect of its overexpression was. Using Mp specific antibody we detected Mp on the surface of the cardiac cells and found that it accumulated to a high level in both *Hand>mblRNAi* and *Hand>Bru3* DM1 lines. We also tested whether the *in silico* identified *dmiR-1* seed site was required for the regulation of Mp expression and confirmed that *Mp* is a direct *in vivo* target of *dmiR-1* in cardiac cells. Consistent with its role downstream of *dmiR-1,* Mp overexpression in the heart mimicked the *dmiR-1* knockdown phenotype, leading to a significantly enlarged heart with reduced contractility. Moreover, genetic rescue experiments with heart-specific attenuation of Mp expression in the *Hand>Bru3* DM1 context reduced heart dilation and ameliorated DCM phenotype in aged flies, thus demonstrating that increased Mp levels contribute to DCM observed in DM1 flies. Previous reports (Louzao-Martinez et al., 2016; Gil-Cayuela et al., 2016) revealed increased expression levels of different collagens associated with DCM in both animal models and patients. Here, we report evidence that Col 15A1 is specifically up-regulated at both transcript and protein levels in cardiac samples from DM1 patients and in particular in those with DCM. Altogether, the observations that Col15A1 expression level is abnormally elevated in DCM-developing DM1 patients and that attenuation of its *Drosophila* ortholog Mp could ameliorate the DCM phenotype suggest that Col15A1 could be a novel therapeutic target in DM1.

DCM, a complex cardiac condition with a poor prognosis in DM1

A large number of genes have so far been implicated in DCM, attesting to the complex molecular origin of this cardiac condition. For example, in *Drosophila,* DCM was observed in mutants of genes encoding contractile and structural muscle proteins such as Troponin I (TpnI), Tropomyosin 2 (Tm2), δ-sarcoglycan and Dystrophin but also associated with deregulations of EGF, Notch, Cdc42 and CCR4-Not signalling pathway components (reviewed in Wolf, 2012). In humans, DCM-causing mutations were also identified in a large number of genes including those encoding cytoskeletal proteins such as FLNC, nuclear membrane protein LMNA or involved in sarcomere stability (Titin, TNNT2, MYH7, TPM1) but also RNA binding protein RBM20 (McNally and Mestroni, 2017).

Here, we focused on DCM associated with DM1. A previous study on a mouse model overexpressing CELF1 and developing DCM (Wang et al., 2015), identified down-regulation of *Transcription factor A mitochondrial* (*Tfam*), *Apelin* (*Apln*) and *Long-chain-fatty-acid-CoA ligase 1* (*Acsl1*) as potentially associated with DCM. It was suggested that CELF1 might regulate their mRNA stability by binding to their 3′UTR regions and causing destabilisation and degradation of their transcripts (Chang Kuei-Ting et al., 2017). In this DCM-developing mouse DM1 model, Col15a transcripts were elevated (Wang et al., 2015), but the role of Col15a in DCM was not analysed. Here, using *Drosophila* DM1 models with a DCM phenotype, we identified up-regulation of Col15A1 ortholog Mp as a molecular determinant of DM1-associated DCM. We also link reduced *miR-1* levels in DCM-developing DM1 cardiac cells to the up-regulation of Mp, establishing that *Mp* is an *in vivo* target of *miR-1*.

Importantly, our findings show that in DM1 patients, Collagen 15A1 is up-regulated in the hearts of patients with DCM. In DM1 patients, the DCM phenotype appears several years after onset and is less common than the conduction system defects and arrhythmias (Lin et al., 1989; Nguyen et al., 1988). However, it is frequently associated with poor prognosis and indication for heart transplant (Papa et al., 2018).

In summary, we report evidence for the importance of *miR-1*-dependent gene deregulations in DM1 and identify *Mp* as a new *miR-1* target involved specifically in DM1-associated DCM. We also demonstrate that Mbl depletion and Bru3 up-regulation in the heart have overlapping impacts on DM1 pathogenesis, both leading to reduced *miR-1*, up-regulation of Mp, and so to DCM (see scheme in Fig. 4C).

Our conclusion is that in a physiological context, Mp level is moderately triggered by Mbl-dependent regulation of *dmiR-1* processing and Bru-3-dependent regulation of *dmiR-1* stability. However, in the DM1 context, Mbl is sequestered in nuclear foci while Bru-3 levels increase, leading to a reduced *dmiR-1* and the up-regulation of its target gene *Mp*. Considering the known role of Mp as a positive regulator of cardiac lumen size (Harpaz et al., 2013) we would expect Mp accumulation in the adult heart also to promote heart tube enlargement, leading to the DCM phenotype. Whether like in embryos this Mp function involves the Slit/Robo signalling pathway remains to be investigated, but the finding that Robo2 is among identified *miR-1* targets up-regulated in DCM-developing DM1 flies (Table 1) supports this possibility. Finally, the fact that Mp ortholog Col15A1 is highly elevated in cardiac samples from DM1 patients with DCM and that reducing Mp ameliorates DCM phenotype in DM1 fly models suggests that Mp/Col15A1 could be an attractive diagnostic and/or therapeutic target for DM1-associated DCM.

MATERIALS AND METHODS

Drosophila stocks

All *D. melanogaster* stocks were grown and crossed at 25° C on standard fly food. In this study, we used three *Drosophila* DM1 models: *UAS-960CTG* (Picchio et al., 2013), *UAS-MblRNAi* (28732, VDRC Vienna, Austria) and *UAS-Bru3* (Harvard: d09837). For *dmiR-1* loss and gain of function we used *UAS-sponge dmiR-1* (Fulga et al., 2015) and *UAS-dmiR-1* (41125, Bloomington, USA) respectively. For functional analyses of Mp, we used *UAS-MpRNAi-TRIP* (52981, Bloomington, USA) and *UAS-3HNC1* (Meyer and Moussian, 2009). For testing the rescue of dilated cardiomyopathy observed in *Hand>Bru3* line, we have recombined *UAS-Bru3* with *UAS-MpTRIP* line to generate *UAS-MpTRIP; Bru3* line. The *UAS-Bru3* line was also recombined with the *UAS-UPRT* (UAS-HA-UPRT Bloomington 27604) line to generate *UAS-Bru3; UPRT* as a negative control for this rescue experiment.

All inducible lines were crossed with the driver line *Hand-Gal4* (provided by Laurent Perrin, TAGC, Marseille, France) to induce the expression of transgenes specifically in the fly heart (cardioblasts and pericardial cells). Control lines were generated by crossing the above-cited lines with w^{1118} line. w^{1118} is a mutant strain with a recessive white-eye phenotype.

Heartbeat analyses of adult *Drosophila* hearts

Physiological analyses of adult *Drosophila* hearts were performed on one and five weeks old female flies using the SOHA approach protocol of Ocorr (Ocorr et al., 2009). For each genotype, about 20 flies were analyzed. First, we proceeded to dissection and preparation of semi-dissected hearts: adult *Drosophila* flies were anesthetized with Fly Nap for 5 minutes, then placed, dorsal side down, into a petri dish coated with a thin layer of petroleum jelly. The head, the ventral thorax and the ventral abdominal cuticle were removed in order to expose the abdominal contents. The ovaries and other organs as well as fats were then removed in order to expose heart tube attached to the dorsal cuticle. Dissection was performed in an oxygenated, artificial hemolymph (AH) solution composed of 108mM Na^+, 5mM KCl, 2mM $CaCl_2$, 8mM $MgCl_2$, 1mM NaH_2PO_4, 4mM $NaHCO_3$, 10mM sucrose, 5mM trehalose, 5mM HEPES (pH 7.1, all reagents from Sigma Chemicals). The solution was oxygenated by air-bubbling for 15 to 20 min. The beating hearts were filmed by a digital camera on 30 seconds movie with speed of 150 frames /second (Digital camera C9300, Hamamatsu, McBain

Instruments, Chatsworth, CA) using microscope Zeiss (Axiophot, Zeiss) using immersion objective 10X. The heartbeats were recorded in A3 and A4 segments. The SOHA program based on Matlab R2009b software has been used for film analysis: The cardiac tube membrane during maximum diastole (relaxation) and maximum systole (contraction) were defined manually. One pair of marks identified the diastolic diameter, and one pair identified the systolic diameter**.** From this vertical row of pixels, a M-mode was generated to analyze the contraction and relaxation intervals: diastolic (DD), and systolic (SD) diameters, heart period (HP), and systolic (SI) and diastolic (DI) intervals. The diastolic and systolic diameters was used to calculate the Fractional shortening (FS) using the formula: (((Diastolic diameter - Systolic diameter)/Diastolic diameter) x 100) (Ocorr et al., 2009).

Immuno-fluorescence staining of *Drosophila* heart

The adult hearts from one and five weeks old females were dissected as described previously, then fixed with formaldehyde 4%. Samples were incubated with primary rat anti-Mp antibodies (1/100) (Harpaz et al., 2013) or goat anti-GFP (1/500) (Abcam ab5450) overnight at 4 °C followed by 3 washes with PBS-Tween 0.1%, of 10 min each, then secondary antibodies anti-rat Alexa-CY3 (1/150) or with anti-goat Alexa-488 (1/150) (Jackson ImmunoResearch), respectively, for two hours at room temperature, Rhodamine phalloidin (1/1000) (Thermo Fischer Scientific) was used to reveal actin filaments. The preparations were mounted in a the Vectashield with DAPI (Vector laboratories, Inc. Burlingame, CA). Immunofluorescence labeled preparations were analyzed using a confocal microscope Leica SP8.

Quantification of Multiplexin immunolabeling

Fluorescent-labelled heart tissues were all processed and stained under the same conditions. The level of fluorescent signal was quantified using ImageJ software by CTCF (Corrected Total Cell Fluorescence) approach. CTCF is calculated according to the formula: Measured by the software Integrated Optical Density - (Area of select x mean fluorescence of background readings). For each heart, CTCF was measured in two regions from segment A3 and two regions from segment A4 with the same areas for the 4 regions. For each genotype 9

hearts were analyzed for cardioblasts with 4 measurements in regions for each, and 3 pericardial cells were analyzed from each heart.

Single molecule fluorescence in situ hybridisation (smFISH)

For detection of *dmiR-1*, flies one and five weeks old were dissected and fixed for 30 min with 4% paraformaldehyde; rinsed at PBS1X -Tween 0.1% three-time, 5 min each. Samples were dehydrated through a series of increasing ethanol concentrations, transferred sequentially to 25%, 50%, 75%, 100% ethanol baths for 10 min each. After removing ethanol tissues were rehydrated through a series of decreasing ethanol concentrations, transferred sequentially 50%, 25% ethanol baths for 10 min each, and then post fixed for 30 min with 4% paraformaldehyde. Then incubated with solution composed of 50% PBT and 50% hybridisation buffer (5 mL Formamide, 0.5 mL SSC 20X, 100 µL ssDNA, 20 µL tRNA 50 ng/ µL, 5 µL Heparin 100 ng/µL, 10 µL Tween) for 5 min. The samples were finally incubated with hybridisation solution for 1h30 min at 50°C. The hybridisation mix including specific DIG-labeled probes (1nM for U6 snRNA positive control ref 339459, 20nM for negative control scramble ref 339459 and 40 nM for DME-miR1-3p ID: 339111) were added in each tube and samples were incubated at 50°C overnight. To remove non-specific RNA hybridisation, samples were washed with ISH (5 mL Formamide, 0.5 mL SSC 20X, 100 µL ssDNA, 5 µL Heparin 100 ng/µL, 10 µL Tween) for 30 min each at 50°C then with PBT. Slides were blocked in western blockage reagent (3mL blockage reagent+ 12mL PBT) for 30 min, incubated with sheep anti-DIG POD antibodies (11633716001, Roche) for 2 hours, treated with the TSA Plus Cyanine 3 System 1% (PerkinElmer, USA) for 5 min, blocked in 20% NGS diluted in PBT for 30 min. Finally, samples were incubated with primary antibodies (anti-Actin 1/250) overnight at 4 °C and then with secondary antibodies coupled with Alexa448 (1/150). The preparations were mounted in a Vectashield with DAPI medium. Immunofluorescence labeling preparations have been then analyzed using a confocal microscope Leica SP8.

***sm*FISH quantification**

Stained *Drosophila* hearts were imaged in 3D to allow the quantification of RNA transcripts in the total volume of cardiac and pericardial cells. The transcripts hybridized with *sm*FISH probes appears on the images as luminous fluorescent spots. The 3D images were analyzed using Imaris (version 9.3.1) that allows the detection, the visualization of spatial distribution as well as the quantification of intensity for each spot detected. To detect the real RNA spots

of interest we have adjusted the threshold of intensity detection according to scramble. To determine the lower threshold in pericardial cells, we have analyzed the spots detected in 27 pericardial cells in 9 heart preparations labelled by scramble. We adjusted the lower treshold above the mean intensity of scramble spots (30) and the upper threshold (255) by default. With this background subtracting parameter, Imaris software generated *dmiR1* spots and calculated the mean intensity for each spot detected as well as the average of the mean intensities for all *dmiR-1* spots. Similar approach has been applied for dmiR-1 smFISH quantification in cardiac cells.

RNA extraction and RT-qPCR on adult fly heart samples

Total RNA was isolated from 20 adult hearts from one and five weeks old female flies, using Direct-zol™RNA Microprep (ref: R2060) from Zymo Research following the manufacturer's instructions. RNA quality and quantity were respectively assessed using Agilent RNA Screen Tape Assay on 4200 TapeStation System (Agilent Technologies) and Qubit RNA HS assay kit on a Qubit 3.0 Fluorometer (Thermo Fischer Scientific). Then, 150 ng total RNA was reverse transcribed using SuperScript IV Reverse Transcriptase kit (Invitrogen) with random primer mix, in a 20 µL reaction. Quantitative PCR was performed in 4 replicates in final volume of 10 µL using Light SYBR Green PCR Master Mix (Roche, Applied Science) on a LightCycler 480 Real-Time PCR System (Roche, Applied Science).
2 µL (3 ng) of cDNA were added to a SYBR Green Master Mix. We used Rp49 as a reference gene. The following pairs of primers were used: *Rp49*: forward GCTTCAAGGGACAGTATCTG and reverse AAACGCGGTTCTGCATGAG; *pre-dmiR-1*: forward TTCAGCCTTTGAGAGTTCCATG and reverse CGCCAGATTTCGCTCCATAC. The relative quantifications of transcripts were obtained with the ΔΔCt method. Finally, nonparametric Mann–Whitney tests were performed to compare control samples and samples of interest.

Generating transgenic fly lines

The *dmiR-1* binding site in 3'UTR of *Mp* was predicted by sequence alignment of 3'UTR *Mp* sequence from flybase (http://flybase.org/) to *dmiR-1* sequence from miRbase (http://www.mirbase.org/) using Bowtie2 (Langmead and Salzberg, 2012). To validate *Mp* as a direct target of *dmiR-1* in *vivo*, we have generated double transgenic fly lines. For the

generation of *UAS-GFP-3'UTRmp* line, approximately 470 base pairs surrounding the predicted *dmiR-1*-target site in 3'UTR of *Mp* were amplified directly from genomic DNA from the w^{1118} flies using the primers Mp-F1: ATAACTAGTTGAGCGGAAACGGAAGGAAGAAGAGGAG and Mp-R1: ATATCTAGATGTTGTGAATGATGACGTTAGG and a high-fidelity DNA Polymerase enzyme (Thermo Scientific Phusion High-Fidelity DNA Polymerase) kit. For the *UAS-GFP-Δ3'UTRmp* line, the same steps were proceeded with primers Mp-F2: ATAACTAGTTGATAAAACAAAACAAATCACAGCAC and Mp-R1: ATATCTAGATGTTGTGAATGATGACGTTAGG to amplify about 350 bp without predicted *dmiR-1*-target site. The *Spe*I and *Xba*I restriction sites were incorporated into primers and introduced by PCR. PCR products were purified using NucleoSpin Plasmid clean up kit after validation of inserts by electrophoresis on 1% agarose gel. After digestion of purified *3'UTR Mp* fragments and *pUASP-PL-Venus* vector by *Spe*I and *Xba*I enzymes, we performed ligation between *3'UTR Mp* fragments and the vector using the T4 DNA ligase kit (Invitrogen) according to the manufacturer's instructions. Purified vectors were then microinjected by the Fly Facility platform to generated transgenic lines. Finally, *UAS-GFP-3'UTRMp* and *UAS-GFP-Δ 3'UTRMp* transgenic lines were combined with *UAS-miR-1* (41125, Bloomington, USA) to generate *UAS-GFP-3'UTRMp; UAS-miR-1* and *UAS-GFP-Δ3'UTRMp; UAS-miR-1* respectively and then crossed with the driver line *Hand -GAL4*.

RNA extraction, RT-qPCR, and immunoblot on DM1 hearts

Human ventricular cardiac muscle tissues were obtained at autopsy from 3 DM1 patients and 3 normal controls following informed consent. All experimental protocols were approved by the Institutional Review Board at Osaka University and carried out in accordance with the approved guidelines. Total mRNA was extracted and first-strand complementary DNA synthesized as described previously (Nakamori et al., 2008). RT-qPCR was performed using TaqMan Gene Expression assays (Hs00266332_m1 and 4333760F, Applied Biosystems) on an ABI PRISM 7900HT Sequence Detection System (Applied Biosystems), as described previously (Nakamori et al., 2011). Level of *COL15A1* mRNA was normalized to *18S* rRNA. For protein analysis, cardiac muscle tissues were homogenized in a 10x volume of radioimmunoprecipitation assay buffer (25 mM Tris-HCl; pH 7.5; 150 mM NaCl; 1% NP-40; 1% sodium deoxycholate; and 0.1% sodium dodecyl sulfate) containing a protein inhibitor

cocktail (Sigma-Aldrich). The homogenate was centrifuged for 10 minutes at 10,000g and the supernatant was collected. Equal amounts of protein (40 µg) were separated by sodium dodecyl sulfate–polyacrylamide gel electrophoresis and transferred onto Immobilon-P membranes (Millipore), as previously described (Nakamori et al., 2008). Blots were blocked for nonspecific protein binding with 5% (w/v) nonfat milk and then incubated with a 1:500-diluted antibody against COL15A1 (Thermo Fisher Scientific) or 1:3000-diluted antibody against GAPDH (glyceraldehyde 3-phosphate dehydrogenase) (Sigma-Aldrich). After repeated washings, the membranes were incubated with horseradish peroxidase-conjugated goat anti-rabbit IgG (Thermo Fisher Scientific). The ECL Prime Western Blotting Detection Reagent (Cytiva) and ChemiDoc Touch Imaging System (Bio-Rad) were used to detect the proteins.

Statistics

Nonparametric Mann-Whitney tests were performed to compare control samples and samples of interest of *Drosophila* model and t-test was performed to compare controls to DM1 context from heart samples of DM1 patients. All statistical analyses were performed using GraphPad Prism (version 8.0.1) software. Results are reported with $P<0.05$ considered statistically significant.

References

Auxerre-Plantié, E., Nakamori, M., Renaud, Y., Huguet, A., Choquet, C., Dondi, C., Miquerol, L., Takahashi, M.P., Gourdon, G., Junion, G., Jagla, T., Zmojdzian, M., Jagla, K., 2019. Straightjacket/α2δ3 deregulation is associated with cardiac conduction defects in myotonic dystrophy type 1. eLife 8, e51114. https://doi.org/10.7554/eLife.51114

Chang Kuei-Ting, Cheng Ching-Feng, King Pei-Chih, Liu Shin-Yi, Wang Guey-Shin, 2017. CELF1 Mediates Connexin 43 mRNA Degradation in Dilated Cardiomyopathy. Circulation Research 121, 1140–1152. https://doi.org/10.1161/CIRCRESAHA.117.311281

Dasgupta, T., Ladd, A.N., 2012. The importance of CELF control: molecular and biological roles of the CUG-BP, Elav-like family of RNA binding proteins. Wiley Interdiscip Rev RNA 3, 104–121. https://doi.org/10.1002/wrna.107

De Haro, M. de, Al-Ramahi, I., Jones, K.R., Holth, J.K., Timchenko, L.T., Botas, J., 2013. Smaug/SAMD4A Restores Translational Activity of CUGBP1 and Suppresses CUG-Induced Myopathy. PLOS Genetics 9, e1003445. https://doi.org/10.1371/journal.pgen.1003445

de Haro, M., Al-Ramahi, I., De Gouyon, B., Ukani, L., Rosa, A., Faustino, N.A., Ashizawa, T., Cooper, T.A., Botas, J., 2006. MBNL1 and CUGBP1 modify expanded CUG-induced toxicity in a Drosophila model of myotonic dystrophy type 1. Hum. Mol. Genet. 15, 2138–2145. https://doi.org/10.1093/hmg/ddl137

Eklund, L., Piuhola, J., Komulainen, J., Sormunen, R., Ongvarrasopone, C., Fässler, R., Muona, A., Ilves, M., Ruskoaho, H., Takala, T.E.S., Pihlajaniemi, T., 2001. Lack of type XV collagen causes a skeletal myopathy and cardiovascular defects in mice. Proc Natl Acad Sci U S A 98, 1194–1199.

Fardaei, M., Larkin, K., Brook, J.D., Hamshere, M.G., 2001. In vivo co-localisation of MBNL protein with DMPK expanded-repeat transcripts. Nucleic Acids Res 29, 2766–2771.

Fardaei, M., Rogers, M.T., Thorpe, H.M., Larkin, K., Hamshere, M.G., Harper, P.S., Brook, J.D., 2002. Three proteins, MBNL, MBLL and MBXL, co-localize in vivo with nuclear foci of expanded-repeat transcripts in DM1 and DM2 cells. Hum Mol Genet 11, 805–814. https://doi.org/10.1093/hmg/11.7.805

Fernandez-Costa, J.M., Garcia-Lopez, A., Zuñiga, S., Fernandez-Pedrosa, V., Felipo-Benavent, A., Mata, M., Jaka, O., Aiastui, A., Hernandez-Torres, F., Aguado, B., Perez-Alonso, M., Vilchez, J.J., Lopez de Munain, A., Artero, R.D., 2013. Expanded CTG repeats trigger miRNA alterations in Drosophila that are conserved in myotonic dystrophy type 1 patients. Hum Mol Genet 22, 704–716. https://doi.org/10.1093/hmg/dds478

Fulga, T.A., McNeill, E.M., Binari, R., Yelick, J., Blanche, A., Booker, M., Steinkraus, B.R., Schnall-Levin, M., Zhao, Y., DeLuca, T., Bejarano, F., Han, Z., Lai, E.C., Wall, D.P., Perrimon, N., Van Vactor, D., 2015. A transgenic resource for conditional competitive inhibition of conserved Drosophila microRNAs. Nat Commun 6, 7279. https://doi.org/10.1038/ncomms8279

Garcia-Lopez, A., Monferrer, L., Garcia-Alcover, I., Vicente-Crespo, M., Alvarez-Abril, M.C., Artero, R.D., 2008. Genetic and Chemical Modifiers of a CUG Toxicity Model in Drosophila. PLOS ONE 3, e1595. https://doi.org/10.1371/journal.pone.0001595

Gil-Cayuela, C., Roselló-LLetí, E., Ortega, A., Tarazón, E., Triviño, J.C., Martínez-Dolz, L., González-Juanatey, J.R., Lago, F., Portolés, M., Rivera, M., 2016. New Altered Non-Fibrillar Collagens in Human Dilated Cardiomyopathy: Role in the Remodeling Process. PLoS One 11. https://doi.org/10.1371/journal.pone.0168130

Griffiths-Jones, S., Grocock, R.J., van Dongen, S., Bateman, A., Enright, A.J., 2006. miRBase: microRNA sequences, targets and gene nomenclature. Nucleic Acids Res 34, D140–D144. https://doi.org/10.1093/nar/gkj112

Groh, W.J., Groh, M.R., Saha, C., Kincaid, J.C., Simmons, Z., Ciafaloni, E., Pourmand, R., Otten, R.F., Bhakta, D., Nair, G.V., Marashdeh, M.M., Zipes, D.P., Pascuzzi, R.M., 2008. Electrocardiographic abnormalities and sudden death in myotonic dystrophy type 1. N. Engl. J. Med. 358, 2688–2697. https://doi.org/10.1056/NEJMoa062800

Harpaz, N., Ordan, E., Ocorr, K., Bodmer, R., Volk, T., 2013. Multiplexin Promotes Heart but Not Aorta Morphogenesis by Polarized Enhancement of Slit/Robo Activity at the Heart Lumen. PLOS Genetics 9, e1003597. https://doi.org/10.1371/journal.pgen.1003597

Hermans, M.C., Faber, C.G., Bekkers, S.C., de Die-Smulders, C.E., Gerrits, M.M., Merkies, I.S., Snoep, G., Pinto, Y.M., Schalla, S., 2012. Structural and functional cardiac changes in myotonic dystrophy type 1: a cardiovascular magnetic resonance study. Journal of Cardiovascular Magnetic Resonance 14, 48. https://doi.org/10.1186/1532-429X-14-48

Houseley, J.M., Wang, Z., Brock, G.J.R., Soloway, J., Artero, R., Perez-Alonso, M., O'Dell, K.M.C., Monckton, D.G., 2005. Myotonic dystrophy associated expanded CUG repeat muscleblind positive ribonuclear foci are not toxic to Drosophila. Hum Mol Genet 14, 873–883. https://doi.org/10.1093/hmg/ddi080

Huguet, A., Medja, F., Nicole, A., Vignaud, A., Guiraud-Dogan, C., Ferry, A., Decostre, V., Hogrel, J.-Y., Metzger, F., Hoeflich, A., Baraibar, M., Gomes-Pereira, M., Puymirat, J., Bassez, G., Furling, D., Munnich, A., Gourdon, G., 2012. Molecular, Physiological, and Motor Performance Defects in DMSXL Mice Carrying >1,000 CTG Repeats from the Human DM1 Locus. PLoS Genet 8. https://doi.org/10.1371/journal.pgen.1003043

Ikeda, S., Kong, S.W., Lu, J., Bisping, E., Zhang, H., Allen, P.D., Golub, T.R., Pieske, B., Pu, W.T., 2007. Altered microRNA expression in human heart disease. Physiological Genomics 31, 367–373. https://doi.org/10.1152/physiolgenomics.00144.2007

Isserlin, R., Merico, D., Wang, D., Vuckovic, D., Bousette, N., Gramolini, A.O., Bader, G.D., Emili, A., 2014. Systems analysis reveals down-regulation of a network of pro-survival miRNAs drives the apoptotic response in dilated cardiomyopathy. Mol. BioSyst. 11, 239–251. https://doi.org/10.1039/C4MB00265B

Kalsotra, A., Singh, R.K., Gurha, P., Ward, A.J., Creighton, C.J., Cooper, T.A., 2014. The Mef2 transcription network is disrupted in myotonic dystrophy heart tissue dramatically altering miRNA and mRNA expression. Cell Rep 6, 336–345. https://doi.org/10.1016/j.celrep.2013.12.025

Katoh, T., Hojo, H., Suzuki, T., 2015. Destabilization of microRNAs in human cells by 3′ deadenylation mediated by PARN and CUGBP1. Nucleic Acids Res 43, 7521–7534. https://doi.org/10.1093/nar/gkv669

Koshelev, M., Sarma, S., Price, R.E., Wehrens, X.H.T., Cooper, T.A., 2010. Heart-specific overexpression of CUGBP1 reproduces functional and molecular abnormalities of myotonic dystrophy type 1. Hum. Mol. Genet. 19, 1066–1075. https://doi.org/10.1093/hmg/ddp570

Kura, B., Kalocayova, B., Devaux, Y., Bartekova, M., 2020. Potential Clinical Implications of miR-1 and miR-21 in Heart Disease and Cardioprotection. Int J Mol Sci 21. https://doi.org/10.3390/ijms21030700

Kuyumcu-Martinez, N.M., Wang, G.-S., Cooper, T.A., 2007. Increased steady state levels of CUGBP1 in Myotonic Dystrophy 1 are due to PKC-mediated hyper-phosphorylation. Mol Cell 28, 68–78. https://doi.org/10.1016/j.molcel.2007.07.027

Langmead, B., Salzberg, S.L., 2012. Fast gapped-read alignment with Bowtie 2. Nat Methods 9, 357–359. https://doi.org/10.1038/nmeth.1923

Lee, J.E., Cooper, T.A., 2009. Pathogenic mechanisms of myotonic dystrophy. Biochem Soc Trans 37. https://doi.org/10.1042/BST0371281

Lee, K.-Y., Li, M., Manchanda, M., Batra, R., Charizanis, K., Mohan, A., Warren, S.A., Chamberlain, C.M., Finn, D., Hong, H., Ashraf, H., Kasahara, H., Ranum, L.P.W., Swanson, M.S., 2013. Compound loss of muscleblind-like function in myotonic dystrophy. EMBO Mol Med 5, 1887–1900. https://doi.org/10.1002/emmm.201303275

Lin, A.E., Mitchell, F.M., Fitz, R.W., Doyle, J.J., 1989. Dilated cardiomyopathy in myotonic dystrophy. Journal of the American College of Cardiology 13, 262–263. https://doi.org/10.1016/0735-1097(89)90582-2

Louzao-Martinez, L., Vink, A., Harakalova, M., Asselbergs, F.W., Verhaar, M.C., Cheng, C., 2016. Characteristic adaptations of the extracellular matrix in dilated cardiomyopathy. International Journal of Cardiology 220, 634–646. https://doi.org/10.1016/j.ijcard.2016.06.253

Masuda, A., Andersen, H.S., Doktor, T.K., Okamoto, T., Ito, M., Andresen, B.S., Ohno, K., 2012. CUGBP1 and MBNL1 preferentially bind to 3′ UTRs and facilitate mRNA decay. Sci Rep 2, 209. https://doi.org/10.1038/srep00209

Mathieu, J., Allard, P., Potvin, L., Prévost, C., Bégin, P., 1999. A 10-year study of mortality in a cohort of patients with myotonic dystrophy. Neurology 52, 1658–1662. https://doi.org/10.1212/wnl.52.8.1658

McNally Elizabeth M., Mestroni Luisa, 2017. Dilated Cardiomyopathy. Circulation Research 121, 731–748. https://doi.org/10.1161/CIRCRESAHA.116.309396

Meola, G., Cardani, R., 2015. Myotonic dystrophies: An update on clinical aspects, genetic, pathology, and molecular pathomechanisms. Biochimica et Biophysica Acta (BBA) -

Molecular Basis of Disease, Neuromuscular Diseases: Pathology and Molecular Pathogenesis 1852, 594–606. https://doi.org/10.1016/j.bbadis.2014.05.019

Meyer, F., Moussian, B., 2009. Drosophila multiplexin (Dmp) modulates motor axon pathfinding accuracy. Development, Growth & Differentiation 51, 483–498. https://doi.org/10.1111/j.1440-169X.2009.01111.x

Nakamori, M., Gourdon, G., Thornton, C.A., 2011. Stabilization of expanded (CTG)•(CAG) repeats by antisense oligonucleotides. Mol Ther 19, 2222–2227. https://doi.org/10.1038/mt.2011.191

Nakamori, M., Kimura, T., Kubota, T., Matsumura, T., Sumi, H., Fujimura, H., Takahashi, M.P., Sakoda, S., 2008. Aberrantly spliced alpha-dystrobrevin alters alpha-syntrophin binding in myotonic dystrophy type 1. Neurology 70, 677–685. https://doi.org/10.1212/01.wnl.0000302174.08951.cf

Nguyen, Harold H., Wolfe, J.T., Holmes, D.R., Edwards, W.D., 1988. Pathology of the cardiac conduction system in myotonic dystrophy: A study of 12 cases. Journal of the American College of Cardiology 11, 662–671. https://doi.org/10.1016/0735-1097(88)91547-1

Nguyen, H. H., Wolfe, J.T., Holmes, D.R., Edwards, W.D., 1988. Pathology of the cardiac conduction system in myotonic dystrophy: a study of 12 cases. J. Am. Coll. Cardiol. 11, 662–671.

Ocorr, K., Fink, M., Cammarato, A., Bernstein, S.I., Bodmer, R., 2009. Semi-automated Optical Heartbeat Analysis of Small Hearts. J Vis Exp. https://doi.org/10.3791/1435

Orengo, J.P., Chambon, P., Metzger, D., Mosier, D.R., Snipes, G.J., Cooper, T.A., 2008. Expanded CTG repeats within the DMPK 3′ UTR causes severe skeletal muscle wasting in an inducible mouse model for myotonic dystrophy. PNAS 105, 2646–2651. https://doi.org/10.1073/pnas.0708519105

Papa, A.A., Verrillo, F., Scutifero, M., Rago, A., Morra, S., Cassese, A., Cioppa, N.D., Magliocca, M.C., Galante, D., Palladino, A., Golino, P., Politano, L., 2018. Heart transplantation in a patient with Myotonic Dystrophy type 1 and end-stage dilated cardiomyopathy: a short term follow-up. Acta Myol 37, 267–271.

Pelargonio, G., Russo, A.D., Sanna, T., De Martino, G., Bellocci, F., 2002. Myotonic dystrophy and the heart. Heart 88, 665–670.

Philips, A.V., Timchenko, L.T., Cooper, T.A., 1998. Disruption of splicing regulated by a CUG-binding protein in myotonic dystrophy. Science 280, 737–741. https://doi.org/10.1126/science.280.5364.737

Picchio, L., Legagneux, V., Deschamps, S., Renaud, Y., Chauveau, S., Paillard, L., Jagla, K., 2018. Bruno-3 regulates sarcomere component expression and contributes to muscle phenotypes of myotonic dystrophy type 1. Dis Model Mech 11. https://doi.org/10.1242/dmm.031849

Picchio, L., Plantie, E., Renaud, Y., Poovthumkadavil, P., Jagla, K., 2013. Novel Drosophila model of myotonic dystrophy type 1: phenotypic characterization and genome-wide view of altered gene expression. Hum Mol Genet 22, 2795–2810. https://doi.org/10.1093/hmg/ddt127

Rao Prakash K., Toyama Yumiko, Chiang H. Rosaria, Gupta Sumeet, Bauer Michael, Medvid Rostislav, Reinhardt Ferenc, Liao Ronglih, Krieger Monty, Jaenisch Rudolf, Lodish Harvey F., Blelloch Robert, 2009. Loss of Cardiac microRNA-Mediated Regulation Leads to Dilated Cardiomyopathy and Heart Failure. Circulation Research 105, 585–594. https://doi.org/10.1161/CIRCRESAHA.109.200451

Rasi Karolina, Piuhola Jarkko, Czabanka Marcus, Sormunen Raija, Ilves Mika, Leskinen Hanna, Rysä Jaana, Kerkelä Risto, Janmey Paul, Heljasvaara Ritva, Peuhkurinen Keijo, Vuolteenaho Olli, Ruskoaho Heikki, Vajkoczy Peter, Pihlajaniemi Taina, Eklund Lauri, 2010. Collagen XV Is Necessary for Modeling of the Extracellular Matrix and Its

Deficiency Predisposes to Cardiomyopathy. Circulation Research 107, 1241–1252. https://doi.org/10.1161/CIRCRESAHA.110.222133

Rau, F., Freyermuth, F., Fugier, C., Villemin, J.-P., Fischer, M.-C., Jost, B., Dembele, D., Gourdon, G., Nicole, A., Duboc, D., Wahbi, K., Day, J.W., Fujimura, H., Takahashi, M.P., Auboeuf, D., Dreumont, N., Furling, D., Charlet-Berguerand, N., 2011. Misregulation of miR-1 processing is associated with heart defects in myotonic dystrophy. Nature Structural & Molecular Biology 18, 840. https://doi.org/10.1038/nsmb.2067

Schilling, L., Forst, R., Forst, J., Fujak, A., 2013. Orthopaedic Disorders in Myotonic Dystrophy Type 1: descriptive clinical study of 21 patients. BMC Musculoskelet Disord 14, 338. https://doi.org/10.1186/1471-2474-14-338

Souidi, A., Jagla, K., 2021. Drosophila Heart as a Model for Cardiac Development and Diseases. Cells 10, 3078. https://doi.org/10.3390/cells10113078

Souidi, A., Zmojdzian, M., Jagla, K., 2018. Dissecting Pathogenetic Mechanisms and Therapeutic Strategies in Drosophila Models of Myotonic Dystrophy Type 1. Int J Mol Sci 19, E4104. https://doi.org/10.3390/ijms19124104

Timchenko, L.T., Salisbury, E., Wang, G.-L., Nguyen, H., Albrecht, J.H., Hershey, J.W.B., Timchenko, N.A., 2006. Age-specific CUGBP1-eIF2 complex increases translation of CCAAT/enhancer-binding protein beta in old liver. J Biol Chem 281, 32806–32819. https://doi.org/10.1074/jbc.M605701200

Timchenko, N.A., Wang, G.-L., Timchenko, L.T., 2005. RNA CUG-binding Protein 1 Increases Translation of 20-kDa Isoform of CCAAT/Enhancer-binding Protein β by Interacting with the α and β Subunits of Eukaryotic Initiation Translation Factor 2. J. Biol. Chem. 280, 20549–20557. https://doi.org/10.1074/jbc.M409563200

Vlasova, I.A., Tahoe, N.M., Fan, D., Larsson, O., Rattenbacher, B., Sternjohn, J.R., Vasdewani, J., Karypis, G., Reilly, C.S., Bitterman, P.B., Bohjanen, P.R., 2008. Conserved GU-rich elements mediate mRNA decay by binding to CUG-binding protein 1. Mol. Cell 29, 263–270. https://doi.org/10.1016/j.molcel.2007.11.024

Wang, E.T., Ward, A.J., Cherone, J.M., Giudice, J., Wang, T.T., Treacy, D.J., Lambert, N.J., Freese, P., Saxena, T., Cooper, T.A., Burge, C.B., 2015. Antagonistic regulation of mRNA expression and splicing by CELF and MBNL proteins. Genome Res 25, 858–871. https://doi.org/10.1101/gr.184390.114

Wang, G.-S., Kearney, D.L., De Biasi, M., Taffet, G., Cooper, T.A., 2007. Elevation of RNA-binding protein CUGBP1 is an early event in an inducible heart-specific mouse model of myotonic dystrophy. J Clin Invest 117, 2802–2811. https://doi.org/10.1172/JCI32308

Wei, Y., Peng, S., Wu, M., Sachidanandam, R., Tu, Z., Zhang, S., Falce, C., Sobie, E.A., Lebeche, D., Zhao, Y., 2014. Multifaceted roles of miR-1 s in repressing the fetal gene program in the heart. Cell Research 24, 278–292. https://doi.org/10.1038/cr.2014.12

Wolf, M.J., 2012. Modeling Dilated Cardiomyopathies in Drosophila. Trends Cardiovasc Med 22, 55–61. https://doi.org/10.1016/j.tcm.2012.06.012

Yu, Z., Teng, X., Bonini, N.M., 2011. Triplet Repeat–Derived siRNAs Enhance RNA–Mediated Toxicity in a Drosophila Model for Myotonic Dystrophy. PLOS Genetics 7, e1001340. https://doi.org/10.1371/journal.pgen.1001340

Tables

Table 1. List of *in silico* identified dmiR-1 targets up-regulated in DM1 contexts developing DCM.

Hand>mblRNAi			Hand>Bru3		
	Symbol	Db id		Symbol	Db id
CG10045	GstD1	FBgn0001149	CG10036	otp	FBgn0015524
CG10650	CG10650	FBgn0046302	CG10076	spir	FBgn0003475
CG10693	slo	FBgn0003429	CG1044	dos	FBgn0016794
CG11125	CG11125	FBgn0033174	CG10650	CG10650	FBgn0046302
CG11128	slif	FBgn0037203	CG10693	slo	FBgn0003429
CG1128	alpha-Est9	FBgn0015577	CG10843	Cyp4p3	FBgn0033397
CG11340	pHCl-2	FBgn0039840	CG11253	Zmynd10	FBgn0266709
CG12287	pdm2	FBgn0004394	CG11319	Dpp10	FBgn0031835
CG12400	ND-B14.5B	FBgn0031505	CG11426	CG11426	FBgn0037166
CG12974	CG12974	FBgn0037065	CG12443	ths	FBgn0033652
CG13323	CG13323	FBgn0033788	CG13253	cmpy	FBgn0037015
CG13796	CG13796	FBgn0031939	CG13648	tnc	FBgn0039257
CG1414	bbx	FBgn0024251	CG13796	CG13796	FBgn0031939
CG1449	zfh2	FBgn0004607	CG13936	CNMa	FBgn0035282
CG14642	CG14642	FBgn0037222	CG14509	jus	FBgn0039647
CG14669	CG14669	FBgn0037326	CG14535	CG14535	FBgn0031955
CG14823	CG14823	FBgn0035734	CG14853	CG14853	FBgn0038246
CG14996	Chd64	FBgn0035499	CG14895	Pak3	FBgn0044826
CG15532	hdc	FBgn0010113	CG15312	CG15312	FBgn0030174
CG16757	Spn	FBgn0010905	CG1667	Sting	FBgn0033453
CG17375	CG17375	FBgn0031861	CG16820	CG16820	FBgn0032495
CG17716	tei	FBgn0000633	CG16995	CG16995	FBgn0031412
CG17875	Cyp9f3	FBgn0038034	CG1722	CG1722	FBgn0031168
CG17928	CG17928	FBgn0032603	CG17224	CG17224	FBgn0031489
CG18188	Damm	FBgn0033659	CG17228	pros	FBgn0004595
CG18211	betaTry	FBgn0010357	CG17264	CG17264	FBgn0031490
CG18480	CG18480	FBgn0028518	CG17907	Ace	FBgn0000024
CG1887	dsb	FBgn0035290	CG18188	Damm	FBgn0033659
CG2381	Syt7	FBgn0039900	CG1916	Wnt2	FBgn0004360
CG2471	Sclp	FBgn0030357	CG2105	Corin	FBgn0033192
CG2543	Fpgs	FBgn0030407	CG2381	Syt7	FBgn0039900
CG2718	Gs1	FBgn0001142	CG3038	CG3038	FBgn0040373
CG30489	Cyp12d1-p	FBgn0050489	CG31127	Wsck	FBgn0046685
CG30502	fa2h	FBgn0050502	CG31221	CG31221	FBgn0051221
CG32490	cpx	FBgn0041605	CG3151	Rbp9	FBgn0010263

CG33307	CG33307	FBgn0053307
CG34026	CG34026	FBgn0054026
CG34405	NaCP60E	FBgn0085434
CG3764	CG3764	FBgn0036684
CG3989	Paics	FBgn0020513
CG42340	CG42340	FBgn0259242
CG4257	Stat92E	FBgn0016917
CG42674	CG42674	FBgn0261556
CG42751	CG42751	FBgn0261805
CG42807	CG42807	FBgn0261989
CG43374	Cht6	FBgn0263132
CG43427	smash	FBgn0263346
CG43690	fok	FBgn0263773
CG44325	CG44325	FBgn0265413
CG45017	IP3K2	FBgn0283680
CG5065	CG5065	FBgn0034145
CG5481	robo2	FBgn0002543
CG5548	ND-B18	FBgn0030605
CG5744	Frq1	FBgn0030897
CG7106	lectin-28C	FBgn0040099
CG7272	CG7272	FBgn0036501
CG7345	Sox21a	FBgn0036411
CG7503	Con	FBgn0005775
CG7727	Appl	FBgn0000108
CG8112	CG8112	FBgn0037612
CG8345	Cyp6w1	FBgn0033065
CG8663	nrv3	FBgn0032946
CG8942	NimC1	FBgn0259896
CG9369	m	FBgn0002577
CG9552	rost	FBgn0011705
CG9734	glob1	FBgn0027657
CG9772	Skp2	FBgn0037236
CG9908	disco	FBgn0000459

CG31795	IA-2	FBgn0031294
CG32183	Ccn	FBgn0052183
CG32191	CG32191	FBgn0052191
CG32521	Mnr	FBgn0052521
CG32602	Muc12Ea	FBgn0052602
CG33307	CG33307	FBgn0053307
CG33542	upd3	FBgn0053542
CG33950	trol	FBgn0284408
CG34220	CG34220	FBgn0085249
CG34256	CG34256	FBgn0085285
CG34361	Dgk	FBgn0085390
CG34405	NaCP60E	FBgn0085434
CG3764	CG3764	FBgn0036684
CG3953	Invadolysin	FBgn0086359
CG3997	RpL39	FBgn0023170
CG40160	CG40160	FBgn0058160
CG4058	Nep4	FBgn0038818
CG42333	Sytbeta	FBgn0261090
CG42450	CG42450	FBgn0259927
CG42540	CG42540	FBgn0260657
CG42543	Mp	FBgn0260660
CG42575	NaPi-III	FBgn0260795
CG42732	SLO2	FBgn0261698
CG42751	CG42751	FBgn0261805
CG42803	gpp	FBgn0264495
CG42807	CG42807	FBgn0261989
CG42817	Ca-Ma2d	FBgn0261999
CG43079	nrm	FBgn0262509
CG43224	Gfrl	FBgn0262869
CG43374	Cht6	FBgn0263132
CG43744	bru3	FBgn0264001
CG43756	Slob	FBgn0264087
CG43901	CG43901	FBgn0264502
CG44085	CG44085	FBgn0264894
CG45017	IP3K2	FBgn0283680
CG4587	stol	FBgn0028863
CG5065	CG5065	FBgn0034145
CG5295	bmm	FBgn0036449
CG5399	CG5399	FBgn0038353
CG5446	CG5446	FBgn0032429
CG5481	robo2	FBgn0002543
CG5744	Frq1	FBgn0030897
CG6220	CG6220	FBgn0033865

	CG6330	CG6330	FBgn0039464
	CG6658	Ugt302K1	FBgn0040251
	CG6713	Nos	FBgn0011676
	CG7191	CG7191	FBgn0031945
	CG7220	CG7220	FBgn0033544
	CG7503	Con	FBgn0005775
	CG7576	Rab3	FBgn0005586
	CG7727	Appl	FBgn0000108
	CG8250	Alk	FBgn0040505
	CG8502	Cpr49Ac	FBgn0033725
	CG8663	nrv3	FBgn0032946
	CG8785	CG8785	FBgn0033760
	CG9552	rost	FBgn0011705
	CG9652	Dop1R1	FBgn0011582
	CG9717	CG9717	FBgn0039789
	CG9907	para	FBgn0285944

Figure legends

Figure 1. Heart-targeted *dmiR-1* attenuation causes DCM in *Drosophila*. (A) Control (*UAS_dmiR-1 sponge*) and **(B)** mutant (*Hand>dmiR-1 sponge*) adult hearts from one-week-old flies labelled for F-actin (red). **(A', B')** Cross-sections of cardiac tubes 3D-reconstructed using Imaris software. M-mode records from one-week-old control (*UAS_ dmiR-1 sponge*) **(C)** and *dmiR-1KD* (*Hand>dmiR-1 sponge*) **(C')** flies showing increased diastolic (green) and systolic diameters (red) in the *dmiR-1KD* context **(C)**.Diastolic **(D)** and systolic **(E)** diameters and cardiac contractility analyses **(**percent fractional shortening) **(F)** performed using SOHA approach for control (*UAS_dmiR-1 sponge*) and *dmiR-1KD* (*Hand>sponge dmiR-1*) contexts at ages one (red) and five (black) weeks. *n* = 20 hearts. Scale bar = 20 µm.

Figure 2. DM1 flies develop DCM phenotype with a reduced *dmiR-1* level in cardiac cells. Cardiac tube size (diastolic **(A, D)** and systolic **(B, E)** diameters) and contractility (percent fractional shortening **(C, F)**) analyses performed using SOHA approach for controls (*UAS_Bru3* and *UAS_mblRNAi*) and DM1 contexts (*Hand>Bru3* and *Hand>mblRNAi*), at ages one (red) and five (black) weeks. *n* = 20 hearts. Representative spot views generated using Imaris from *in situ* hybridisations with miRCURY LNA probe for *dmiR-1* and used for

quantification of *dmiR-1* levels. Spot views of *dmiR-1* in hearts of one-week-old control (*UAS_mblRNAi*) **(G)** and DM1 flies (*Hand>mblRNAi*) **(G')** are shown. The zoom region corresponds to area used for smFISH quantifications. **(H, I)** Scatter plot graph showing the signal intensity quantified in cardioblasts of one- (red) and five- (black) week-old flies for controls (*UAS_Bru3*, *UAS_mblRNAi*) and DM1 contexts (*Hand>Bru3*, *Hand>mblRNAi*). *n* = 9 hearts. Scale bar = 40 µm

Figure 3. Multiplexin, a new cardiac *dmiR-1* target is up-regulated in DCM-developing DM1 flies. (A) Up-regulated genes identified by heart-specific transcriptomic approach (TU-tagging (Auxerre-Plantié et al., 2019) in DM1 contexts developing DCM (top Venn diagrams) underwent *in silico* screening for *miR-1* binding sites leading to identification of a set of potential *dmiR-1*-targets up-regulated in DM1 (lower Venn diagrams), of which *Multiplexin* with *miR-1* binding site in its 3'UTR region (*miR-1* seed site alignment) **(B)**. dmiR-1 binding site in *3'UTRMp* region is required to negatively regulate Mp expression *in vivo*. Adult hearts from transgenic GFP-sensor lines carrying *3'UTRMp* region with (*UAS_GFP 3'UTRMp)* or without *dmiR-1* seed site (*UAS_GFP* Δ*3'UTRMp*)**.** These lines were combined with the *UAS-dmiR1* line to generate double transgenic lines and tested for GFP expression in non-targeted context **(C,E)** or in heart-targeted context **(D,F)** after crossing with cardiac Hand-Gal4 driver. When heart-targeted, GFP expression in *Hand>GFP 3'UTRMp; dmiR1* line (carrying *dmiR-1* seed site) **(D')** is attenuated compared to *Hand>GFP* Δ*3'UTRMp; dmiR-1* line (lacking dmiR-1 seed site) **(F')**. Scale bar = 40 µm. (**C)** Cross sections of adult hearts from one- and five-week-old controls (*UAS_mblRNAi*, *UAS_Bru3*) **(G,H,I,J)** and DM1 contexts (*Hand>mblRNAi*, *Hand>Bru3*) **(G',H',I',J')** labelled for Mp (green). Highlighted regions correspond to areas used for quantifications of the fluorescent signals **(G)**. **(K,L)** Graphs of Mp signal quantification in cardioblasts from adult flies aged one and five weeks for controls (*UAS_mblRNAi*, *UAS_Bru3*) and DM1 contexts (*Hand>mblRNAi*, *Hand>Bru3*) using CTCF method. *n* = 9 hearts. Scale bar = 10 µm

Figure 4. Heart-targeted Mp overexpression leads to DCM. (A) Adult heart aged one week **(A,B)** and its cross sections **(C,D)** labelled for Mp (green) and actin (red) for controls (*UAS_Mp*) and Mp overexpression context (*Hand>Mp*). Cardiac variables (diastolic **(E)** and systolic **(F)** diameters) and percent fractional shortening **(G)** for control (*UAS_Mp*) and Mp overexpression (*Hand>Mp)* conditions at ages one (red) and five weeks (black); *n* = 20 hearts. Scale bar = 5 µm. M-modes representing cardiac variables in five-week-old control

(H) and Mp-overexpressing **(H')** flies. **(I)** Scheme presenting cardiac role of *dmiR-1* and its target *Mp* in DCM-developing *Drosophila* DM1 models. In wild-type *Drosophila* heart Mbl promotes *pre-dmiR-1* processing. Bru-3 has potential antagonistic role in the destabilisation of *dmiR1*. As a result, in this context *dmiR-1* and its target Mp levels are moderate. In DM1, Mbl is sequestered and Bru-3 is stabilised, causing inefficient processing of *pre-dmiR1* and destabilisation of mature *dmiR-1*. As a result, in the DM1 context, the *dmiR-1* level is reduced while its target Mp level is high. This leads to an enlarged heart with adversely affected contractility.

Figure 5. Increased cardiac expression of human Mp ortholog Col15A1 is associated with DCM in DM1 patients. (A) *Col15A1* transcript levels tested by RT-QPCR and **(B)** Col15A1 protein levels tested by Western blot in cardiac samples from healthy donors and from DM1 patients with and without DCM. Cardiac variables (diastolic **(C)** and systolic **(D)** diameters and percent fractional shortening **(E)**) assessed by SOHA approach for control 1 (*UAS-MpRNAi; UAS-Bru3)*, control 2 (*UAS-Bru3; UAS-UPRT*), Mp rescue (*Hand>MpRNAi; Bru3*) and DM1 context (*Hand>Bru3; UPRT*) at age five weeks. *n* = 20 hearts. Cross-sections of cardiac tubes 3D-reconstructed using Imaris software from five-week-old Control 1 (*UAS-MpRNAi; UAS-Bru3*) **(F)**, DM1 (*Hand>Bru3; UPRT*) **(G) and** Mp rescue (*Hand>MpRNAi; Bru3*) **(H)** flies labeled with actin. Scale barre = 20 µm

Figure 1

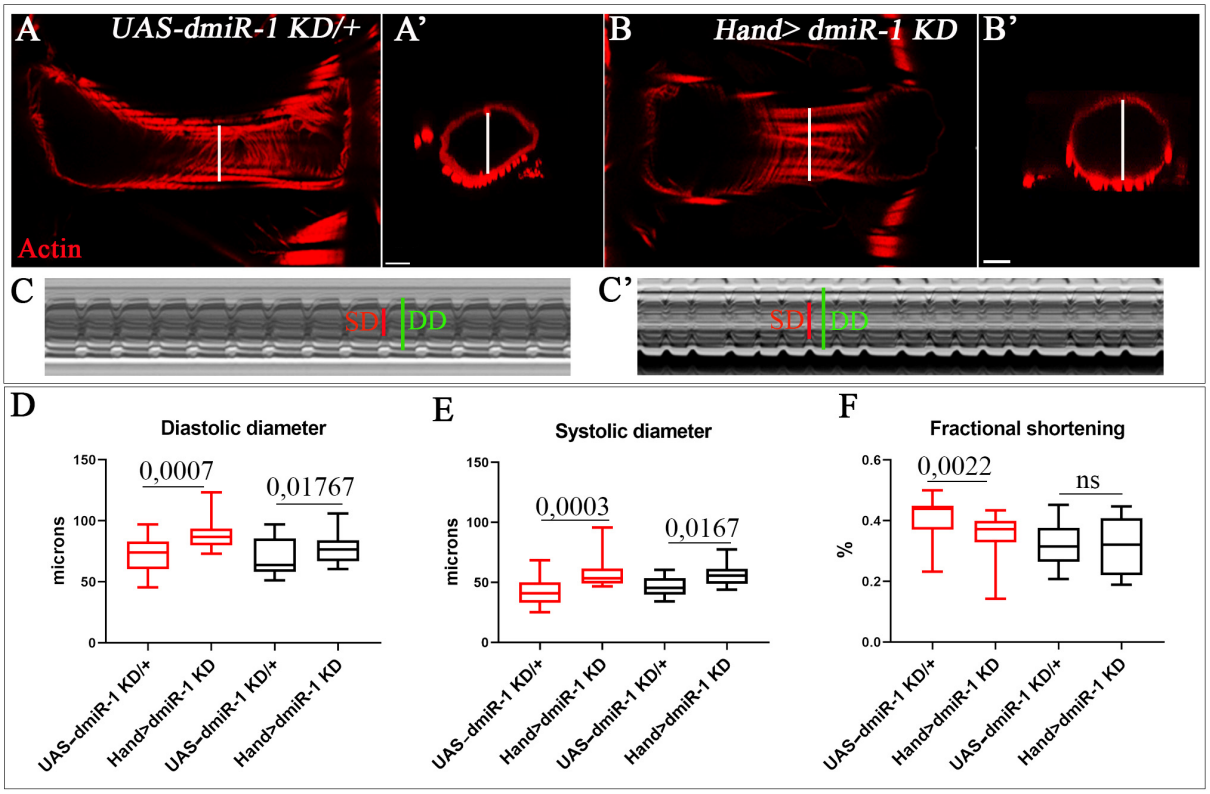

Figure 2

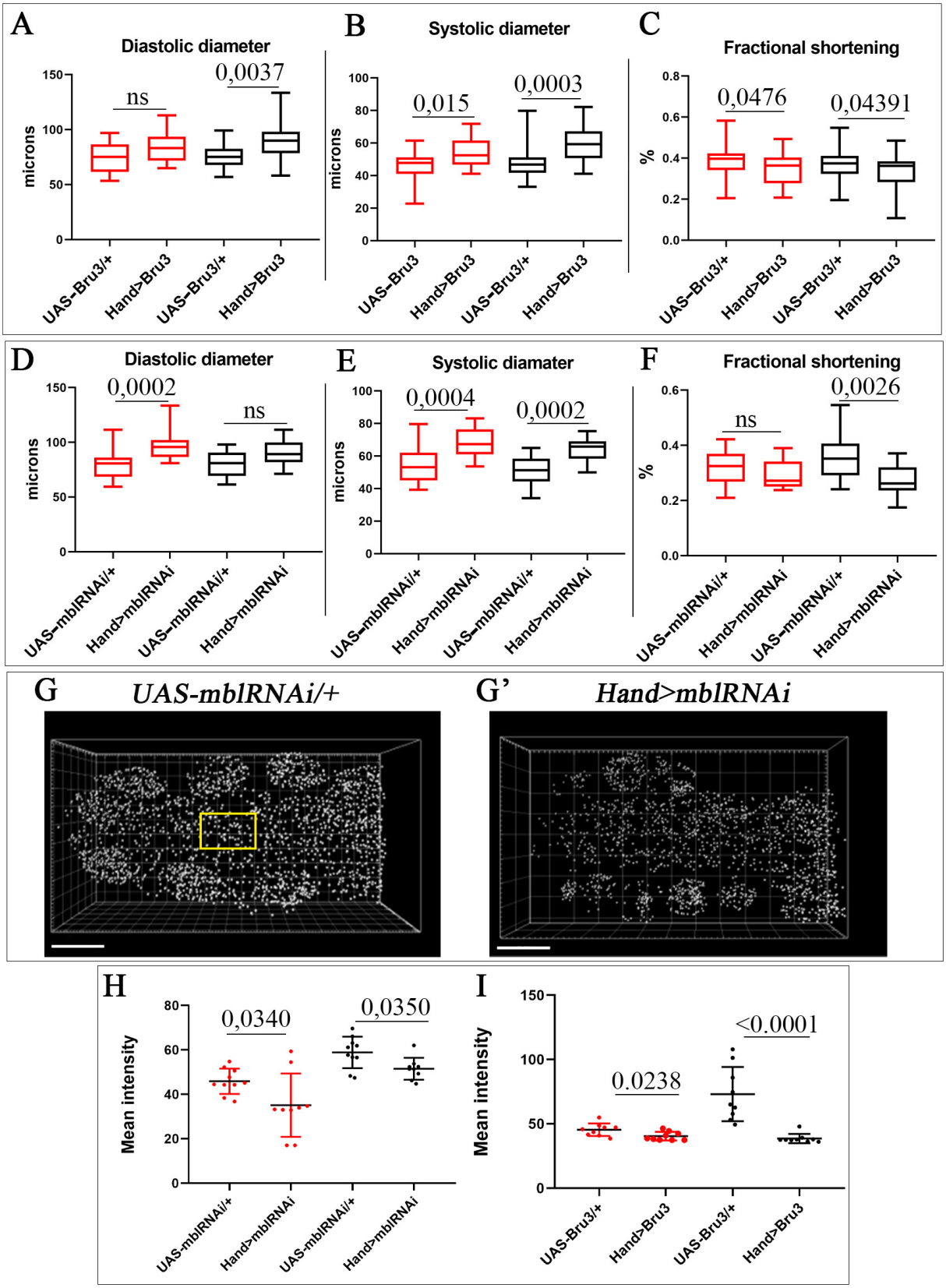

Figure 3

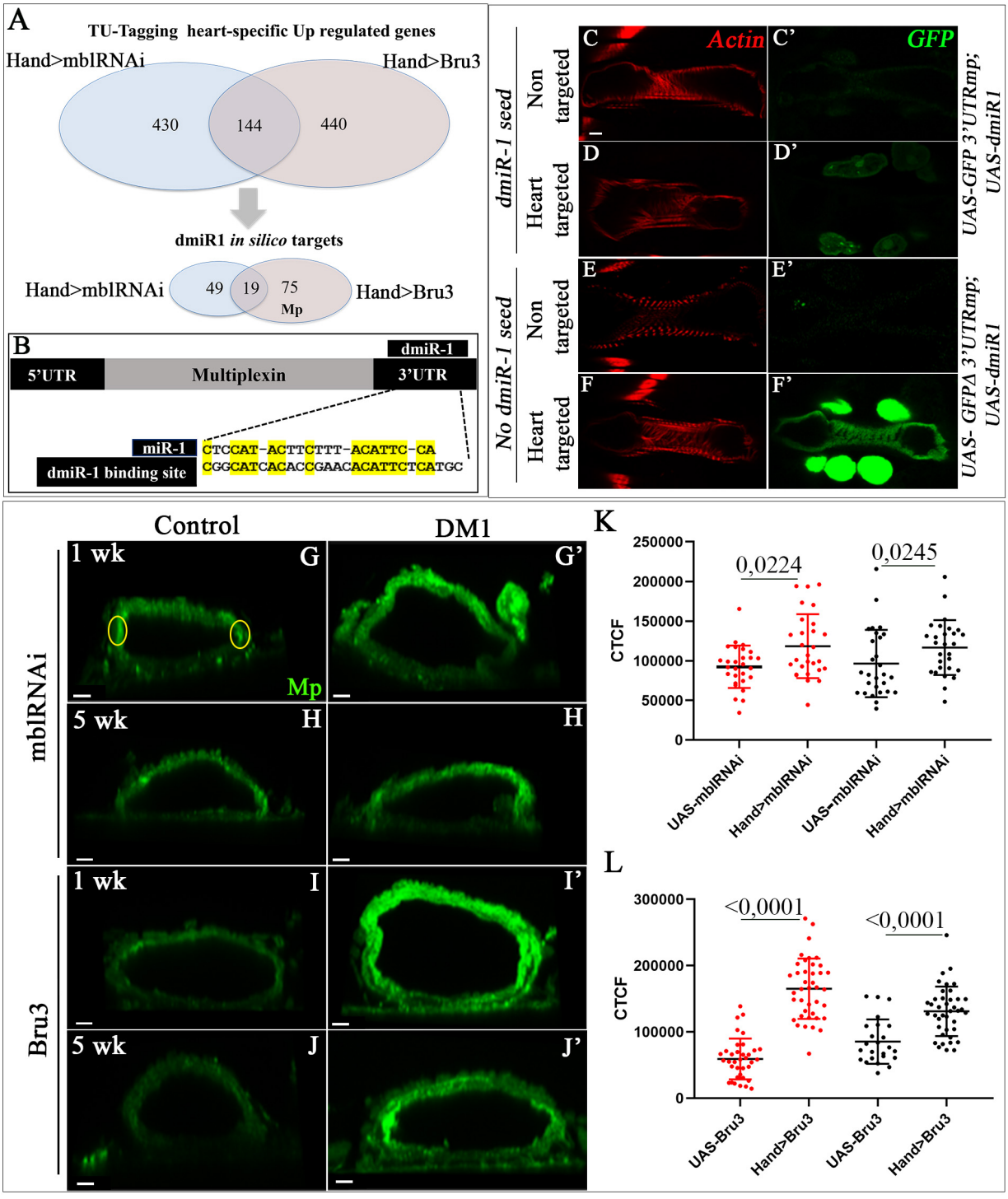

Figure 4

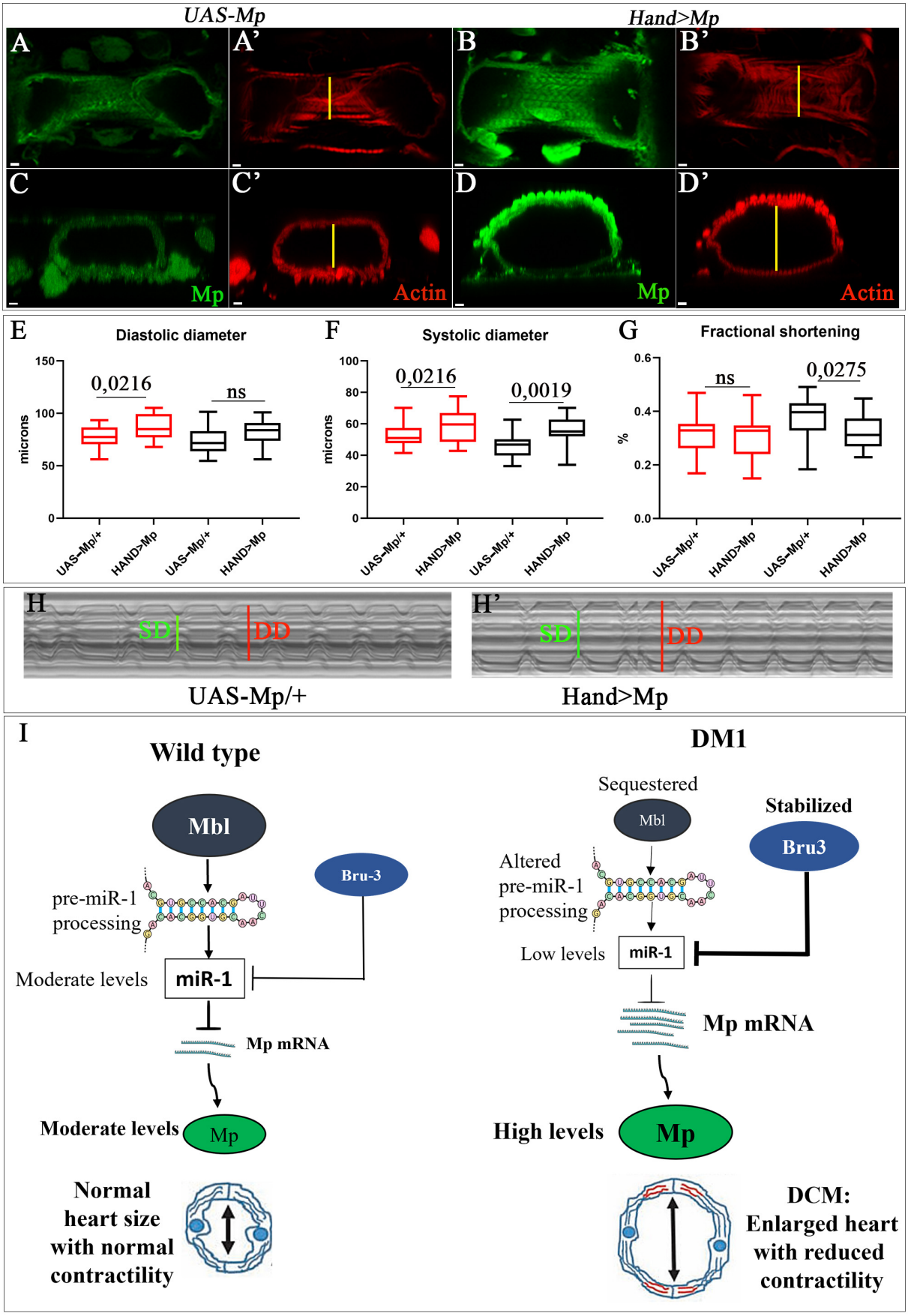

Figure 5